The Impact of Edema on MRI-Radiomics for the Prediction of Lung Metastasis in Soft Tissue Sarcoma.

Roberto Casale , Riccardo De Angelis , Nicolas Coquelet , Ayoub Mokhtari * , Maria Antonietta Bali

Posted Date: 17 August 2023

doi: 10.20944/preprints202308.1234.v1

Keywords: Radiomics; magnetic resonance imaging (MRI); soft tissue sarcoma; lung metastasis; edema

Article

The Impact of Edema on MRI-Radiomics for the Prediction of Lung Metastasis in Soft Tissue Sarcoma

Roberto Casale, Riccardo De Angelis †, Nicolas Coquelet †, Ayoub Mokhtari * and Maria Antonietta Bali

Institut Jules Bordet, Université Libre de Bruxelles, 1070 Brussels, Belgium

* Correspondence: ayoub.mokhtari@ulb.be

† These two authors contributed equally to this work.

Highlights

- This study assessed the predictive capabilities of radiomic features extracted from the edema and tumoral mass of soft tissue sarcomas in predicting lung metastasis.
- Both the models utilizing edema-related features and the model utilizing mass-related features demonstrated promising results in predicting the occurrence of lung metastasis, with similar performances.
- The findings suggest that the analysis of radiomic features extracted exclusively from edema can offer valuable insights into the prediction of lung metastasis.

Abstract: Introduction: This study aimed to evaluate whether radiomic features extracted solely from the edema of soft tissue sarcomas (STS) could predict the occurrence of lung metastasis in comparison with features extracted solely from the tumoral mass. Materials and Methods: We retrospectively analyzed magnetic resonance imaging (MRI) scans of 32 STSs including 14 with lung metastasis and 18 without. Segmentation of the tumor mass and edema was performed for each MRI examination. A total of 107 radiomic features were extracted for each mass segmentation and 107 radiomic features for each edema segmentation. A two-step feature selection process was applied. Two predictive features for the development of lung metastasis were selected from the mass-related features, as well as two predictive features from the edema-related features. Two random forest models were created based on these selected features; 100 random subsampling runs were performed. Key performance metrics including accuracy and area under the ROC curve (AUC) were calculated, and the resulting accuracies were compared. Results: The model based on mass-related features achieved a median accuracy of 0.83 and a median AUC of 0.88, while the model based on edema-related features achieved a median accuracy of 0.75 and a median AUC of 0.79. Statistical analysis comparing the accuracies of the two models revealed no significant difference. Conclusion: Both models showed promise in predicting the occurrence of lung metastasis in soft tissue sarcomas. These findings suggest that radiomic analysis of edema features can provide valuable insights into the prediction of lung metastasis in soft tissue sarcomas.

Keywords: radiomics; magnetic resonance imaging (MRI); soft tissue sarcoma; lung metastasis; edema

1. Introduction

Soft-tissue sarcomas (STSs) encompass a diverse range of malignancies originating from mesenchymal cells. The World Health Organization recognizes more than 50 distinct subtypes within this category. STSs are rare tumors, accounting for approximately 1% of all cancer cases [1]. Despite their low incidence, they pose significant concerns due to their potential for distant metastases, which occur in about 25% of cases and contribute to the majority of deaths; high-grade STSs can exhibit a metastatic rate of up to 50% [2–4]. The lungs are the most common site of metastasis, accounting for around 80% of lesions [5].

 doi:10.20944/preprints202308.1234.v1

The prognosis for patients who develop metastases is generally poor. Those who undergo surgical metastasectomy have a 3-year survival rate of less than 50%, while patients who are not eligible for surgery have a survival rate below 20%. The median survival time following the diagnosis of distant metastasis is approximately 11.6 months [2]. The identification of patients with a heightened susceptibility to develop distant metastasis holds the potential to enhance the efficacy of therapeutic interventions [6,7].

In a study conducted by White [8], the presence of satellite tumor cells was observed in 10 out of 15 patients with STSs. Among these cases, tumor cells were detected within the edema zone as visualized on magnetic resonance imaging (MRI) in 9 patients.

By thoroughly investigating the edema, researchers can gain valuable insights into the intricate interactions between the tumor and its surrounding tissue. The edema is closely interconnected with the tumor microenvironment, which encompasses factors such as inflammation, angiogenesis, and tissue remodeling. This comprehensive analysis of the edema can provide additional prognostic information beyond relying solely on tumor volume. The incorporation of edema analysis in the evaluation of STSs has the potential to aid in patient risk stratification and facilitate personalized treatment decisions.

Despite the significance of edema in the tumor microenvironment, there is a notable gap in the existing literature. Our literature search on PubMed using the keywords [("soft tissue sarcoma" OR "soft tissue sarcoma") AND edema] revealed a lack of studies specifically focused on radiomic features extracted solely from the edema. Therefore, the primary objective of our study is to fill this gap by investigating the potential correlations between radiomic features derived from the edema of STSs and the occurrence of lung metastases.

Through this exploration, our study aims to uncover the prognostic value and clinical significance of these radiomic features in relation to lung metastases in STS patients. By elucidating the role of edema-related radiomic features, we can advance our understanding of STSs and improve patient management strategies. This investigation may also lead to the identification of biomarkers associated with tumor behavior and response. Ultimately, our study seeks to contribute valuable knowledge to the field and enhance the care provided to STS patients.

2. Materials and Methods

2.1. Dataset

For our study, we employed an open-source anonymized database as the principal data repository (http://doi.org/10.7937/K9/TCIA.2015.7GO2GSKS); this comprehensive dataset consisted of 51 cases of STSs affecting the extremities, which were histologically confirmed [7,9]. Each patient in the dataset had undergone fluoro-D-glucose positron emission tomography and MRI scans as part of their evaluation, conducted between November 2004 and November 2011.

It is important to note that the MRI protocols employed were not standardized across all patients. To ensure consistency in our analysis, we specifically selected T2-weighted fat-saturated (T2FS) or short tau inversion recovery (STIR) MRI scans. Patients were categorized into two groups based on clinical outcomes: "no lung metastases" (group A) and "lung metastases" (group B).

Inclusion criteria required that the selected examinations exhibit distinct segmentations for both the tumor mass and tumor mass plus the associated edema, while excluding cases where the two segmentations were identical (e.g., cases with no observable edema). In other studies, T2FS and STIR images are deemed comparable in terms of texture analysis, therefore we grouped them together as a single category [7,10].

Following these criteria, a total of 32 patients were included in our analysis.

2.2. Segmentation and Feature Extraction

Segmentations for the examinations were acquired from the aforementioned publicly available database. Each individual segmentation underwent visual evaluation by a radiologist with eight

Preprints (www.preprints.org) | NOT PEER-REVIEWED | Posted: 17 August 2023 doi:10.20944/preprints202308.1234.v1

years of experience, and modifications were made as deemed necessary. The 3D Slicer software, version 4.13, was employed for this process [11].

For every exam, the following segmentations were considered:

- Gross Tumoral Volume (GTV): segmentation that encompassed only the tumor mass;
- Edema Tumoral Volume (EDV): segmentation obtained by subtracting the segmentation of tumor mass alone from the segmentation of tumor mass and edema (Figure 1).

The computation of all radiomic features was performed using Pyradiomics 3.0.1 (https://pyradiomics.readthedocs.io), a software library designed for the extraction of radiomic features from medical imaging data [12]. Additionally, a Python script developed by the authors was utilized, ensuring compliance with the Image Biomarker Standardisation Initiative (IBSI) standard [13].

The hyperparameters for feature extraction were set with the following values: normalize = True; removeOutliers = 3; binCount = 50; resampledPixelSpacing = 0.8,0.8,5.5; interpolator = sitk.sitkBSpline; correctMask = True. All other parameters were kept at their default values. For each examination, features were extracted individually from each exam in a separate manner.

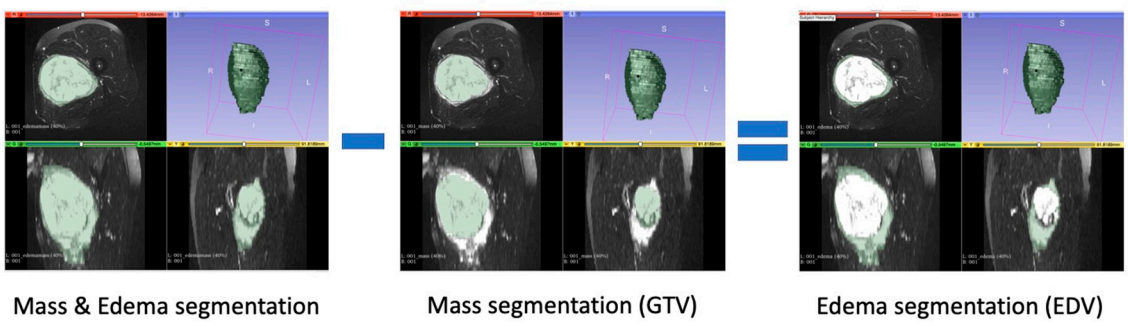

Figure 1. GTV and EDV segmentations; EDV segmentations were obtained by subtracting the GTV segmentation from the segmentation of tumor mass and edema.

The radiomic features extracted in this study were categorized into seven main groups: First Order (FOF) Features; Shape Features (SHAPE); Gray Level Co-occurrence Matrix (GLCM) Features; Gray Level Run Length Matrix (GLRLM) Features; Gray Level Size Zone Matrix (GLSZM) Features; Gray Level Dependence Matrix (GLDM) Features; Neighbouring Gray Tone Difference Matrix (NGTDM) Features. The definitions and a detailed list of these features can be found in the Pyradiomics feature documentation, available at https://pyradiomics.readthedocs.io.

2.3. Feature Selection

Initially, highly correlated features were removed by applying the Spearman correlation coefficient, discarding those with a correlation value exceeding 0.8.

Subsequently, the process encompassed evaluating all possible feature combinations, starting from individual features and gradually increasing the combination size up to a maximum of five features. For each combination size, we applied the Exhaustive Feature Selection algorithm [14] to systematically assess all combinations and calculate the average area under the ROC curve (AUC) score using 5-fold cross-validation and a Random Forest (RF) classifier. In brief, the feature selection process was iterated for each combination size, and for each iteration, the combination exhibiting the highest average AUC score was chosen as the best combination for that specific number of features.

Lastly, the number and names of the final selected features corresponded to the first peak value observed in the average AUC score (avg_score) considering the best combinations ranging from 1 to 5 features.

 doi:10.20944/preprints202308.1234.v1

2.4. Modeling and Statistical Analysis

A RF model based on selected GTV features (RF-GTV) and a RF model based on selected EDV features (RF-EDV) were compared. In particular, we performed 100 random subsampling iterations to evaluate the performance of the two models. For each iteration, we randomly split the dataset into training and testing sets; as suggested by Nadeau and Bengio [15] the training set was five times larger than the testing set.

The RF models were trained on the training sets and evaluated on the corresponding testing sets. Performance metrics such as accuracy, sensitivity, specificity, and AUC were computed for both algorithms.

The median and interquartile range (IQR) of accuracy, sensitivity, specificity, and AUC were calculated across the 100 iterations for both RF-GTV and RF-EDV models.

To compare the two models, it was used the Nadeau and Bengio's corrected resampled t-test for the obtained accuracies. According to [16], 100 random subsampling and the Nadeau and Bengio's corrected resampled t-test ensure appropriate Type I error control, low Type II error, and high replicability, enabling reliable comparisons between the algorithms.

The Spearman correlation coefficient was employed to calculate the inter-correlation among the selected features. Additionally, the Mann-Whitney test was utilized to assess statistically significant differences in selected feature values between group A / group B.

The described pipeline was performed with Python 3.7 version. For RF, max_depth (the longest path from the root node to the leaf node) was set to 10 were; the default values were retained for all remaining parameters.

3. Results

3.1. Dataset

Our study comprised a cohort of 32 patients, consisting of 14 males and 18 females, with a median age of 60 years (range: 16-83 years). Throughout the follow-up period, 18 patients remained free from lung metastases (group A), while 14 patients experienced lung metastases (group B).

The median duration from diagnosis to the last follow-up was 684.5 days (range: 377-1329 days) for group A, whereas the median duration from diagnosis to the onset of metastases or local recurrence was 162 days (range: 29-731 days) for group B.

Regarding histological grade, 18 patients had high-grade sarcoma (8 patients in group A and 10 patients in group B), 13 patients had intermediate-grade sarcoma (10 patients in group A and 3 patients in group B), and 1 patients had low-grade sarcoma (in group A). Further details on relevant clinical parameters and treatment modalities can be found in Table 1, along with the supplementary information provided in the Supplementary table section under "Clinical data".

Table 1. Clinical parameters.

	Group A (No lung metastasis)	**Group B (Lung metastasis)**
Number of patients	18	14
Gender ratio (M/F)	5/13	9/5
Age, y, median (range)	53.5 (16-83)	62.5 (44-74)
Grade ratio (Low/Intermediate/High)	1/9/8	0/4/10

The MRI protocols were heterogeneous; T2FS or STIR sequences were used. Additional details regarding the MRI acquisition protocols can be found in the Supplementary table section under "MRI data". Not all individual patients had both STIR and T2FS sequences available. Consequently, we selected the only fluid-sensitive sequence that was accessible for each patient during the analysis[7,10].

 doi:10.20944/preprints202308.1234.v1

3.2. Features Extraction and Selection

After conducting a visual evaluation, it was determined that the segmentations of 31 exams were suitable for both GTV and EDV; however, in one exam, manual adjustments were made to improve the delineation of the EDV segmentation.

A comprehensive set of 214 radiomics features was extracted, specifically comprising 107 features from the EDV segmentation and 107 features from the GTV segmentation.

In relation to the features extracted from GTV and EDV, after the removal of highly correlated features, a total of 31 features were retained for GTV and 33 EDV. Subsequently, the Exhaustive Feature Selection algorithm was iteratively applied, considering the range of 1 to 5 features, and identifying the first peak in the average AUC score. As a result, 2 features were selected for both GTV and EDV, as shown in Table 2.

Table 2. Selected features for Gross Tumor Volume (GTV) and Edema Tumor Volume (EDV).

Selected features	
Gross Tumor Volume (GTV)	**Edema Tumor Volume (EDV)**
original_glcm_Correlation	original_firstorder_Kurtosis
original_glszm_SmallAreaLowGrayLevelEmphasis	original_glszm_SizeZoneNonUniformityNormalized

3.3. Classification Performance

After conducting 100 random subsampling iterations for both the RF-GTV and RF-EDV models, the resulting performance metrics are shown in Table 3; in particular accuracy was 0.83 for RF-GTV and 0.75 for RF-EDV.

Based on the results of the Nadeau and Bengio's corrected resampled t-test, there was no statistically significant difference observed between the accuracies of the two models (p-value = 0.441).

The ROC curves and AUC values for both models are depicted in Figure 2.

Table 3. Classification performance on 100 random subsampling iterations.

	RF-GTV median [interquartile range]	**RF-EDV median [interquartile range]**
Accuracy	0.83 [0.17]	0.75 [0.17]
Sensitivity	0.67 [0.50]	0.67 [0.50]
Specificity	1.00 [0.33]	0.80 [0.33]
AUC	0.88 [0.23]	0.79 [0.38]

Preprints (www.preprints.org) | NOT PEER-REVIEWED | Posted: 17 August 2023 doi:10.20944/preprints202308.1234.v1

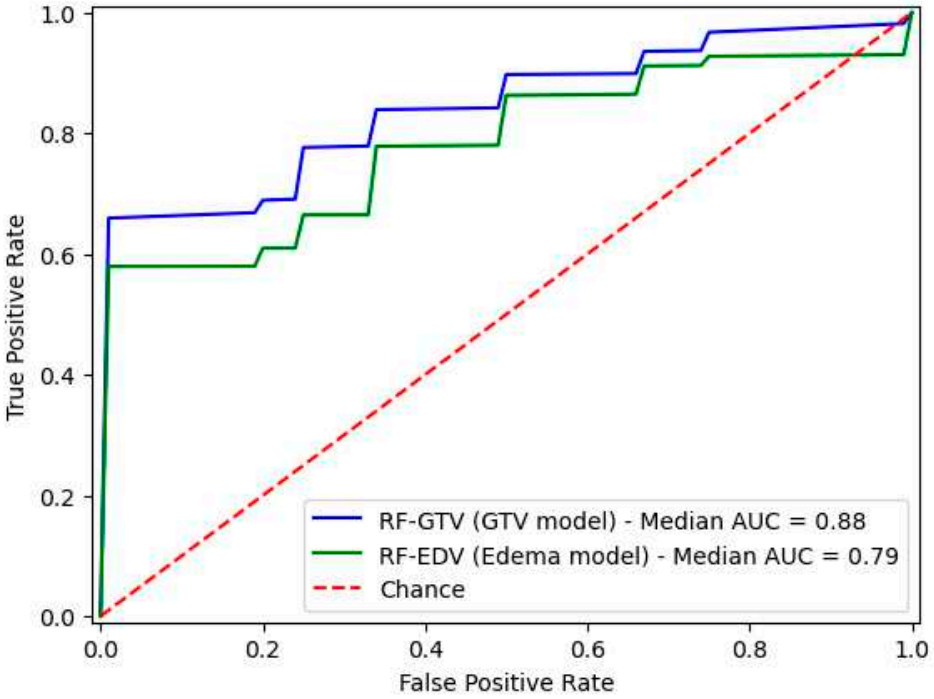

Figure 2. ROCs and AUCs for the RF-GTV (GTV model) and RF-EDV (edema model).

Figure 3: displays the intercorrelation among the selected features, which was computed using the Spearman correlation coefficient. Figures 4 and 5 illustrate the boxplots representing the selected features in group A and group B; the statistical analysis conducted using the Mann-Whitney test revealed no significant differences among the selected features in terms of the comparison between group A and group B.

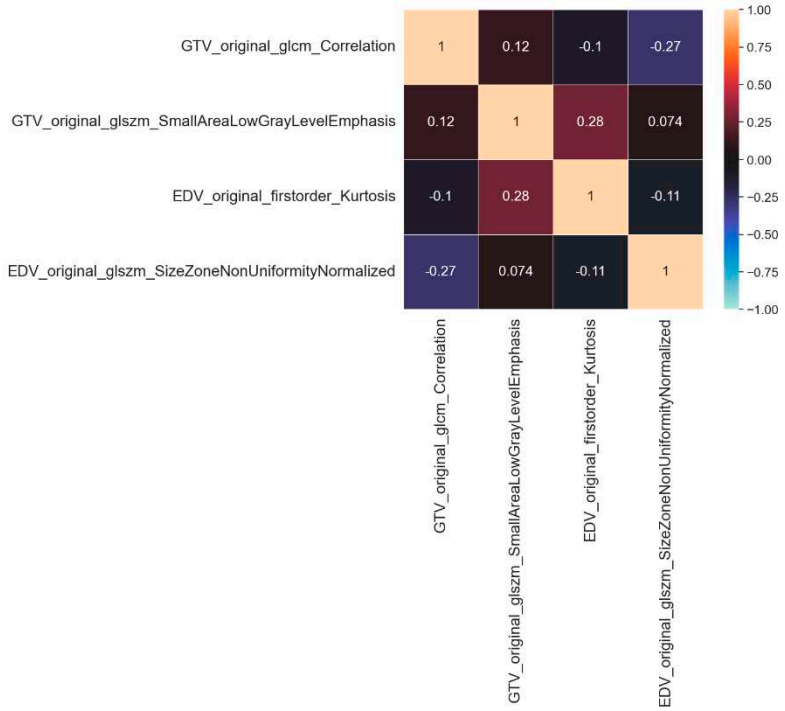

Figure 3. Intercorrelation among the selected features for both Gross Tumor Volume (GTV) and Edema Tumor Volume (EDV).

Preprints (www.preprints.org) | NOT PEER-REVIEWED | Posted: 17 August 2023 doi:10.20944/preprints202308.1234.v1

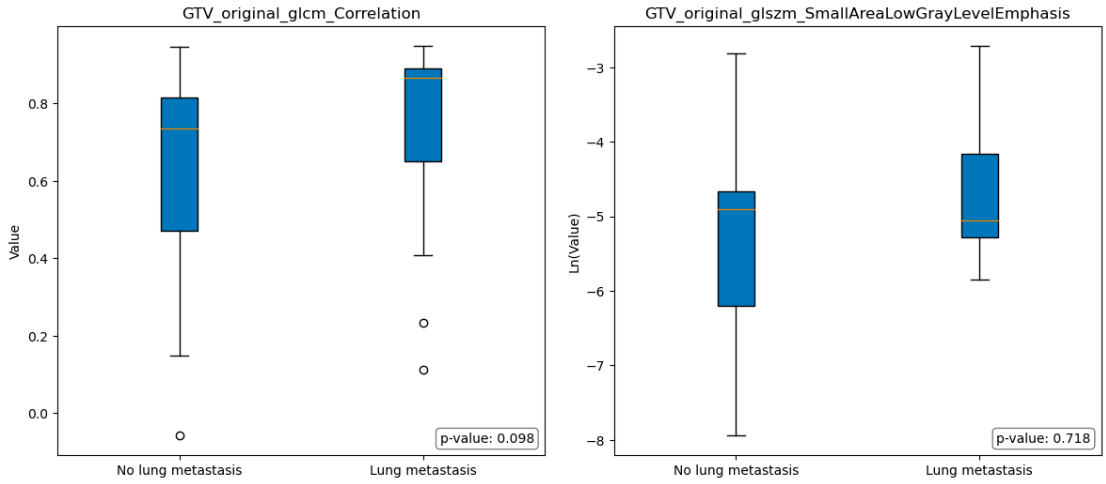

Figure 4. Boxplots for selected features for Gross Tumor Volume (GTV) model; Mann-Whitney p-value for statistically significant differences of value distribution.

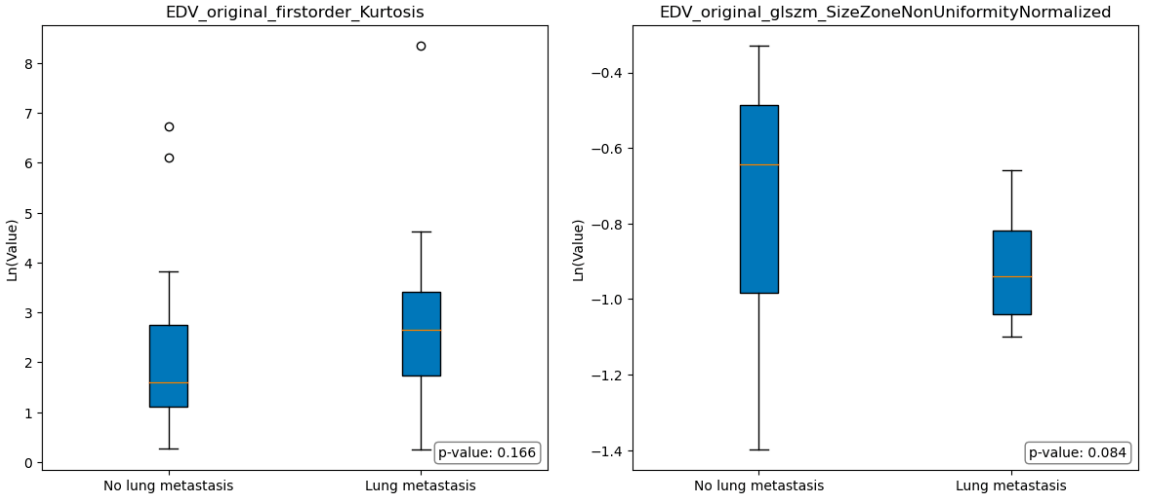

Figure 5. Boxplots for selected features for Edema Tumor Volume (EDV) model; Mann-Whitney p-value for statistically significant differences of value distribution.

4. Discussion

This study aimed to compare the predictive ability of radiomic features extracted from the edema and tumoral mass of STSs in predicting lung metastasis. MRI scans of 32 STSs were retrospectively analyzed, with 18 cases without lung metastasis and 14 cases with lung metastasis. A total of 107 radiomic features were extracted from each GTV and EDV segmentation. After feature selection, the feature vectors contained two features for mass model (original_glcm_Correlation and original_glszm_SmallAreaLowGrayLevelEmphasis) and two features for edema model (original_firstorder_Kurtosis and original_glszm_SizeZoneNonUniformityNormalized). Random forest models were created using the selected features, and key performance metrics were calculated. The model based on mass-related features (RF-GTV) achieved a median accuracy of 0.83 and a median AUC of 0.88, while the model based on edema-related features (RF-EDV) achieved a median accuracy of 0.75 and a median AUC of 0.79. According to the Nadeau and Bengio corrected t-test, statistical analysis showed no significant difference between the accuracies of the two models.

The Spearman correlation coefficient was used to assess the independence of feature vectors within the training dataset; the results indicated that the feature vectors were statistically independent.

 doi:10.20944/preprints202308.1234.v1

In the context of comparing images obtained from the EDV segmentations of individuals without lung metastasis (group A) and those with lung metastasis (group B), some differences were observed, even if not statistically significant. Specifically, Group A exhibited a lower median value of Original FirstOrder Kurtosis, indicating a more peaked distribution of pixel intensities around the mean. Furthermore, Group A exhibited a significantly higher median value of Size-Zone Non-Uniformity Normalized, indicating the presence of regions within the image with varying sizes or distinct patterns.

In other terms, group A images showed a relatively consistent overall texture with localized variations or structures that contribute to the generally heterogeneity of the image. While group B had pronounced variations and irregularities in pixel intensities throughout the region, with regions that exhibited relatively consistent size zones, indicating the presence of distinct histological structures or patterns (e.g. tumor cells arranged in well-defined nests).

To support these findings, the presence of satellite tumor cells within the context of edema and the association of edema and high-grade STSs has been investigated in [8]. Moreover, several previous studies [17–23] have examined various factors on MRI (including edema) and have highlighted the prognostic significance of baseline size, heterogeneous signal intensities on pre-treatment conventional MRI sequences, necrotic signal, peritumoral edema and enhancement, and the presence of a tail sign; these studies have also investigated the associations between these features and the histological grading according to "Fédération National des Centres de Lutte Contre le Cancer" grading system.

Other studies have examined edema [7,22,24–31], but none of these studies have specifically extracted radiomic features solely from the edema region of STSs. In particular, Crombé et al. [22] examined the changes in semantic features before, during, and after neoadjuvant therapy and surgery, using MRI; it was found that changes in edema enhancement were associated with the presence of tumor cells beyond the lesion borders, while variations in edema were associated with disease-free survival; however, none of the outcomes studied were associated with the assessment of edema on baseline MRI. Fadli et al [24] examined the changes in semantic and radiomic features in a cohort of 2 consecutive pre-therapy MRIs; the findings revealed a significant association between the presence or increase of edema (assessed semantically) and the occurrence of local recurrence. In another study [26], selected semantic and radiomic features were analyzed in a cohort of patients who underwent two consecutive MRI scans before and after two cycles of neoadjuvant chemotherapy; the analysis revealed that variations in the surrounding edema (measured semantically) were associated with a positive treatment response, defined as a threshold of less than 10% viable cells on surgical specimens.

The current study has several limitations that need to be acknowledged. Firstly, the sample size used in this study is relatively small, which can reduce the statistical power of the classification outcomes. To mitigate this limitation, we employed 100 random subsampling iterations to assess the performance of the two models. Each iteration involved randomly splitting the dataset into training and testing sets, following the recommendation of Nadeau and Bengio [15], with the training set being five times larger than the testing set. Secondly, the study faced limitations associated with variations in MRI scanning parameters. These differences could potentially introduce batch effects, but they also presented an opportunity to examine the robustness of the methods across diverse image acquisition parameters. Thirdly, we did not employ the De-Long test to compare the AUCs values of the models. We made this decision based on concerns raised about the DeLong method, primarily due to its misuse when training and testing the models using the same dataset [32,33]. Instead, we opted to use the Nadeau and Bengio corrected t-test to compare the accuracies of the models [16].

In summary, both RF-GTV and RF-EDV models exhibited promising potential for predicting the occurrence of lung metastasis in soft tissue sarcomas. Specifically, the model incorporating radiomic features solely extracted from the edema region (RF-EDV) demonstrated the capability to predict lung metastasis, although its performance was slightly inferior to the model based on mass-related

features (RF-GTV). However, the disparity between the two models did not reach statistical significance.

5. Conclusions

These findings suggest that the utilization of radiomic analysis focusing on edema features holds promise in predicting lung metastasis in soft tissue sarcomas, providing results that are comparable to those obtained from mass-related features. Further investigations involving larger cohorts are warranted to validate the clinical utility of these models.

Data Availability Statement: The dataset, the code and the segmentations used in this article can be provided upon contact with the corresponding author.

Abbreviations: Magnetic resonance imaging (MRI); area under the ROC curve (AUC); Soft-tissue sarcoma (STS); T2-weighted fat-saturated (T2FS); short tau inversion recovery (STIR); Gross Tumoral Volume (GTV); Edema Tumoral Volume (EDV); First Order Features (FOF); Shape Features (SHAPE); Gray Level Co-occurrence Matrix Features (GLCM); Gray Level Run Length Matrix Features (GLRLM); Gray Level Size Zone Matrix Features (GLSZM); Gray Level Dependence Matrix Features (GLDM); Neighbouring Gray Tone Difference Matrix Features (NGTDM); Random Forest (RF), Random Forest model based on selected GTV features (RF-GTV); Random Forest model based on selected EDV features (RF-EDV); interquartile range (IQR).

References

1. Kransdorf MJ. Malignant soft-tissue tumors in a large referral population: distribution of diagnoses by age, sex, and location. AJR Am J Roentgenol. 1995;164: 129–134.
2. Billingsley KG, Lewis JJ, Leung DH, Casper ES, Woodruff JM, Brennan MF. Multifactorial analysis of the survival of patients with distant metastasis arising from primary extremity sarcoma. Cancer. 1999;85: 389–395.
3. Brennan MF. Soft tissue sarcoma: advances in understanding and management. Surgeon. 2005;3: 216–223.
4. Stojadinovic A, Leung DHY, Hoos A, Jaques DP, Lewis JJ, Brennan MF. Analysis of the prognostic significance of microscopic margins in 2,084 localized primary adult soft tissue sarcomas. Ann Surg. 2002;235: 424–434.
5. Lewis JJ, Brennan MF. Soft tissue sarcomas. Curr Probl Surg. 1996;33: 817–872.
6. Komdeur R, Hoekstra HJ, van den Berg E, Molenaar WM, Pras E, de Vries EGE, et al. Metastasis in soft tissue sarcomas: prognostic criteria and treatment perspectives. Cancer Metastasis Rev. 2002;21: 167–183.
7. Vallières M, Freeman CR, Skamene SR, El Naqa I. A radiomics model from joint FDG-PET and MRI texture features for the prediction of lung metastases in soft-tissue sarcomas of the extremities. Phys Med Biol. 2015;60: 5471–5496.
8. White LM, Wunder JS, Bell RS, O'Sullivan B, Catton C, Ferguson P, et al. Histologic assessment of peritumoral edema in soft tissue sarcoma. Int J Radiat Oncol Biol Phys. 2005;61: 1439–1445.
9. Clark K, Vendt B, Smith K, Freymann J, Kirby J, Koppel P, et al. The Cancer Imaging Archive (TCIA): maintaining and operating a public information repository. J Digit Imaging. 2013;26: 1045–1057.
10. Zhao W, Huang X, Wang G, Guo J. PET/MR fusion texture analysis for the clinical outcome prediction in soft-tissue sarcoma. Cancer Imaging. 2022;22: 7.
11. Fedorov A, Beichel R, Kalpathy-Cramer J, Finet J, Fillion-Robin J-C, Pujol S, et al. 3D Slicer as an image computing platform for the Quantitative Imaging Network. Magn Reson Imaging. 2012;30: 1323–1341.
12. van Griethuysen JJM, Fedorov A, Parmar C, Hosny A, Aucoin N, Narayan V, et al. Computational Radiomics System to Decode the Radiographic Phenotype. Cancer Res. 2017;77: e104–e107.
13. Zwanenburg A, Vallières M, Abdalah MA, Aerts HJWL, Andrearczyk V, Apte A, et al. The Image Biomarker Standardization Initiative: Standardized Quantitative Radiomics for High-Throughput Image-based Phenotyping. Radiology. 2020;295: 328–338.
14. Raschka S. MLxtend: Providing machine learning and data science utilities and extensions to Python's scientific computing stack. J Open Source Softw. 2018;3: 638.
15. Nadeau C, Bengio Y. Inference for the Generalization Error. Mach Learn. 2003;52: 239–281.
16. Bouckaert RR, Frank E. Evaluating the replicability of significance tests for comparing learning algorithms. Advances in Knowledge Discovery and Data Mining. Berlin, Heidelberg: Springer Berlin Heidelberg; 2004. pp. 3–12.
17. Zhao F, Ahlawat S, Farahani SJ, Weber KL, Montgomery EA, Carrino JA, et al. Can MR imaging be used to predict tumor grade in soft-tissue sarcoma? Radiology. 2014;272: 192–201.

18. Lefkowitz RA, Landa J, Hwang S, Zabor EC, Moskowitz CS, Agaram NP, et al. Myxofibrosarcoma: prevalence and diagnostic value of the "tail sign" on magnetic resonance imaging. Skeletal Radiol. 2013;42: 809–818.
19. Yoo HJ, Hong SH, Kang Y, Choi J-Y, Moon KC, Kim H-S, et al. MR imaging of myxofibrosarcoma and undifferentiated sarcoma with emphasis on tail sign; diagnostic and prognostic value. Eur Radiol. 2014;24: 1749–1757.
20. Trojani M, Contesso G, Coindre JM, Rouesse J, Bui NB, de Mascarel A, et al. Soft-tissue sarcomas of adults; study of pathological prognostic variables and definition of a histopathological grading system. Int J Cancer. 1984;33: 37–42.
21. Fernebro J, Wiklund M, Jonsson K, Bendahl P-O, Rydholm A, Nilbert M, et al. Focus on the tumour periphery in MRI evaluation of soft tissue sarcoma: infiltrative growth signifies poor prognosis. Sarcoma. 2006;2006: 21251.
22. Crombé A, Le Loarer F, Stoeckle E, Cousin S, Michot A, Italiano A, et al. MRI assessment of surrounding tissues in soft-tissue sarcoma during neoadjuvant chemotherapy can help predicting response and prognosis. Eur J Radiol. 2018;109: 178–187.
23. Nakamura T, Matsumine A, Matsubara T, Asanuma K, Yada Y, Hagi T, et al. Infiltrative tumor growth patterns on magnetic resonance imaging associated with systemic inflammation and oncological outcome in patients with high-grade soft-tissue sarcoma. PLoS One. 2017;12: e0181787.
24. Fadli D, Kind M, Michot A, Le Loarer F, Crombé A. Natural Changes in Radiological and Radiomics Features on MRIs of Soft-Tissue Sarcomas Naïve of Treatment: Correlations With Histology and Patients' Outcomes. J Magn Reson Imaging. 2022;56: 77–96.
25. Sedaghat S, Schmitz F, Meschede J, Sedaghat M. Systematic analysis of post-treatment soft-tissue edema and seroma on MRI in 177 sarcoma patients. Surg Oncol. 2020;35: 218–223.
26. Crombé A, Périer C, Kind M, De Senneville BD, Le Loarer F, Italiano A, et al. T -based MRI Delta-radiomics improve response prediction in soft-tissue sarcomas treated by neoadjuvant chemotherapy. J Magn Reson Imaging. 2019;50: 497–510.
27. Tsagozis P, Brosjö O, Skorpil M. Preoperative radiotherapy of soft-tissue sarcomas: surgical and radiologic parameters associated with local control and survival. Clin Sarcoma Res. 2018;8: 19.
28. Wang L, Pretell-Mazzini J, Kerr DA, Chelala L, Yang X, Jose J, et al. MRI findings associated with microscopic residual tumor following unplanned excision of soft tissue sarcomas in the extremities. Skeletal Radiol. 2018;47: 181–190.
29. Bahig H, Roberge D, Bosch W, Levin W, Petersen I, Haddock M, et al. Agreement among RTOG sarcoma radiation oncologists in contouring suspicious peritumoral edema for preoperative radiation therapy of soft tissue sarcoma of the extremity. Int J Radiat Oncol Biol Phys. 2013;86: 298–303.
30. Duy Hung N, Tam N-T, Khanh Huyen D, Thi N-V, Minh Duc N. Diagnostic performance of magnetic resonance imaging in discriminating benign and malignant soft tissue tumors. Int J Gen Med. 2023;16: 1383–1391.
31. Crombé A, Bertolo F, Fadli D, Kind M, Le Loarer F, Perret R, et al. Distinct patterns of the natural evolution of soft tissue sarcomas on pre-treatment MRIs captured with delta-radiomics correlate with gene expression profiles. Eur Radiol. 2023;33: 1205–1218.
32. Chen W, Samuelson FW, Gallas BD, Kang L, Sahiner B, Petrick N. On the assessment of the added value of new predictive biomarkers. BMC Med Res Methodol. 2013;13: 98.
33. Kang L, Chen W, Petrick NA, Gallas BD. Comparing two correlated C indices with right-censored survival outcome: a one-shot nonparametric approach. Stat Med. 2015;34: 685–703.